

# Demonstration of low loss $\beta$ -Ga<sub>2</sub>O<sub>3</sub> optical waveguides in the UV–NIR spectra

Cite as: Appl. Phys. Lett. **115**, 251108 (2019); <https://doi.org/10.1063/1.5133845>

Submitted: 28 October 2019 . Accepted: 04 December 2019 . Published Online: 18 December 2019

 Jingan Zhou,  Hong Chen,  Houqiang Fu,  Kai Fu, Xuguang Deng,  Xuanqi Huang,  Tsung-Han Yang,  Jossue A. Montes, Chen Yang, Xin Qi, Baoshun Zhang, Xiaodong Zhang, and  Yuji Zhao



View Online



Export Citation



CrossMark

## ARTICLES YOU MAY BE INTERESTED IN

[A review of Ga<sub>2</sub>O<sub>3</sub> materials, processing, and devices](#)

Applied Physics Reviews **5**, 011301 (2018); <https://doi.org/10.1063/1.5006941>

[Metal/BaTiO<sub>3</sub>/β-Ga<sub>2</sub>O<sub>3</sub> dielectric heterojunction diode with 5.7 MV/cm breakdown field](#)

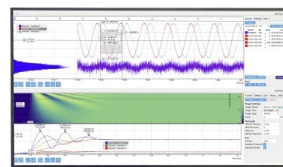
Applied Physics Letters **115**, 252104 (2019); <https://doi.org/10.1063/1.5130669>

[Investigations on band commutativity at all oxide p-type NiO/n-type β-Ga<sub>2</sub>O<sub>3</sub> heterojunction using photoelectron spectroscopy](#)

Applied Physics Letters **115**, 251603 (2019); <https://doi.org/10.1063/1.5126150>

Challenge us.

What are your needs for periodic signal detection?



Zurich Instruments



# Demonstration of low loss $\beta$ -Ga<sub>2</sub>O<sub>3</sub> optical waveguides in the UV–NIR spectra

Cite as: Appl. Phys. Lett. **115**, 251108 (2019); doi: [10.1063/1.5133845](https://doi.org/10.1063/1.5133845)

Submitted: 28 October 2019 · Accepted: 4 December 2019 ·

Published Online: 18 December 2019











View Online



Export Citation



CrossMark

Jingan Zhou,<sup>1</sup>  Hong Chen,<sup>1</sup>  Houqiang Fu,<sup>1</sup>  Kai Fu,<sup>1</sup>  Xuguang Deng,<sup>1</sup> Xuanqi Huang,<sup>1</sup>  Tsung-Han Yang,<sup>1</sup>  Jossue A. Montes,<sup>1</sup>  Chen Yang,<sup>1</sup> Xin Qi,<sup>1</sup> Baoshun Zhang,<sup>2</sup> Xiaodong Zhang,<sup>2,a)</sup> and Yuji Zhao<sup>1,b)</sup> 

## AFFILIATIONS

<sup>1</sup>School of Electrical, Computer and Energy Engineering, Arizona State University, Tempe, Arizona 85287, USA

<sup>2</sup>Key Laboratory of Nanodevices and Applications, Suzhou Institute of Nano-tech and Nano-bionics, CAS, Suzhou 215123, China

<sup>a)</sup>[xdzhang2007@sinano.ac.cn](mailto:xdzhang2007@sinano.ac.cn)

<sup>b)</sup>[Yuji.Zhao@asu.edu](mailto:Yuji.Zhao@asu.edu)

## ABSTRACT

In this paper, we report the fabrication of low loss beta-phase gallium oxide ( $\beta$ -Ga<sub>2</sub>O<sub>3</sub>) optical waveguides and the propagation loss analysis of the waveguides in the ultraviolet (UV) to near infrared (NIR) spectral region. The  $\beta$ -Ga<sub>2</sub>O<sub>3</sub> thin films were grown on sapphire substrates using metal organic chemical vapor deposition and were fabricated into various waveguide structures using nanofabrication processes. A low propagation loss of 3.7 dB/cm was obtained on the  $\beta$ -Ga<sub>2</sub>O<sub>3</sub> waveguide at the wavelength of 810 nm, which is comparable to the state of the art. Combined with theoretical simulations, various loss mechanisms from two-photon absorption, sidewall scattering, top surface scattering, and bulk scattering were discussed for  $\beta$ -Ga<sub>2</sub>O<sub>3</sub> waveguides, and their contributions to the total optical loss were estimated. These results show that  $\beta$ -Ga<sub>2</sub>O<sub>3</sub> is a promising optical material for the fabrication of various integrated photonic devices in the UV–NIR spectra region.

Published under license by AIP Publishing. <https://doi.org/10.1063/1.5133845>

Photonic integrated circuits (PICs) have shown excellent performance in high-speed signal transmission and processing compared with traditional discrete optical components. In the past few years, silicon photonics has attracted considerable attention as an excellent candidate for PICs and has exhibited good compatibility with the mature CMOS processes.<sup>1,2</sup> However, the narrow bandgap (1.1 eV) of silicon restricts the light transmission to wavelengths longer than 1130 nm, which hinders its applications in frequency metrology,<sup>3,4</sup> on-chip mode-locking,<sup>5</sup> visible light communications,<sup>6</sup> spectroscopy,<sup>7</sup> and biosensing,<sup>8</sup> where the transmission of ultraviolet (UV)–near infrared (NIR) spectra is required. To extend the working wavelengths into the visible spectral, other wide-bandgap materials have been investigated, such as silicon nitride with a bandgap of 5.0 eV at 300 K.<sup>9</sup> However, the disadvantage of silicon nitride lies in the strong material absorption due to its N–H bond concentrations,<sup>10</sup> which limits its low-loss applications in the UV–NIR spectra. Recently,  $\beta$ -Ga<sub>2</sub>O<sub>3</sub> has shown many excellent material properties for power device applications as a wide-bandgap material.<sup>11,12</sup> But few investigations were made on its optical properties. In this paper, we are inspired to propose  $\beta$ -Ga<sub>2</sub>O<sub>3</sub> as an optical material platform for PIC applications in the UV–NIR spectral. The wide bandgap of  $\beta$ -Ga<sub>2</sub>O<sub>3</sub> (4.8 eV)<sup>13</sup> provides broadband transparency and a small two-photon coefficient ( $\beta_{\text{TPA}} = 0.6 \text{ cm/GW}$  at

400 nm),<sup>14</sup> which allows for weak photon absorption. Furthermore, it also has a small lattice mismatch with III–N material system,<sup>15</sup> which is beneficial for the active integration of III–N lasers and detectors. Therefore,  $\beta$ -Ga<sub>2</sub>O<sub>3</sub> is promising for integrated photonic applications in the UV–NIR spectral if low propagation loss could be achieved. In this work, we fabricated  $\beta$ -Ga<sub>2</sub>O<sub>3</sub> optical waveguides and performed detail propagation loss analysis for these devices in the UV to NIR spectra region. A low propagation loss of 3.7 dB/cm was obtained on the  $\beta$ -Ga<sub>2</sub>O<sub>3</sub> waveguide at the wavelength of 810 nm, which is comparable to the state of the art. The low loss obtained will open the door for photonic devices based on  $\beta$ -Ga<sub>2</sub>O<sub>3</sub>.

Metal organic chemical vapor deposition (MOCVD) has been investigated and performs well for the  $\beta$ -Ga<sub>2</sub>O<sub>3</sub> thin-film epitaxy.<sup>16</sup> The  $\beta$ -Ga<sub>2</sub>O<sub>3</sub> films in this work were grown on *c*-plane sapphire substrates using MOCVD. High-purity O<sub>2</sub> gas and triethylgallium (TMGa) were utilized as oxygen and gallium sources, respectively. High-purity N<sub>2</sub> was used as the carrier gas for TMGa. The  $\beta$ -Ga<sub>2</sub>O<sub>3</sub> film was grown at 750 °C and 760 Torr. The thickness of the  $\beta$ -Ga<sub>2</sub>O<sub>3</sub> films was measured to be 1  $\mu\text{m}$  using an ellipsometer. The root mean square roughness was measured to be 8.4 nm using an atomic force microscope in a scanning area of 5  $\mu\text{m} \times 5 \mu\text{m}$ . The  $\beta$ -Ga<sub>2</sub>O<sub>3</sub> epilayers were then fabricated into waveguide devices, and the fabrication

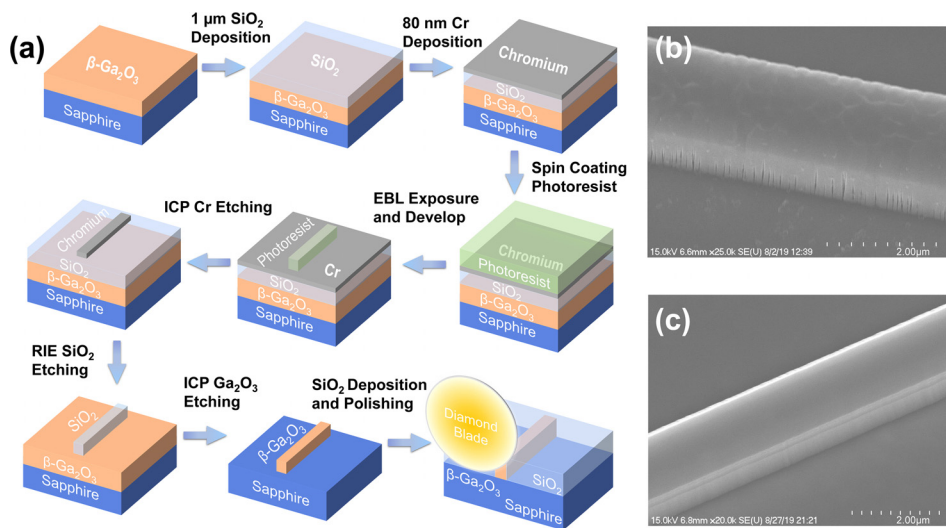


FIG. 1. (a) Schematics of the fabrication process for  $\beta\text{-Ga}_2\text{O}_3$  waveguides. (b) SEM images of waveguide sidewall with unoptimized ICP recipe. (c) SEM images of waveguide sidewall with optimized ICP recipe.

process is illustrated in Fig. 1(a). First,  $1\ \mu\text{m}$  of  $\text{SiO}_2$  film and  $80\ \text{nm}$  of chromium (Cr) film were deposited on a  $\beta\text{-Ga}_2\text{O}_3/\text{Al}_2\text{O}_3$  sample by plasma-enhanced chemical vapor deposition (PECVD) and e-beam evaporation, respectively. A layer of  $290\ \text{nm}$  negative photoresist (maD-2403) was applied onto the Cr layer by spin-coating. The Cr layer served as the hardmask during  $\text{SiO}_2$  etching and a conductive layer for electron beam lithography (EBL). After the EBL exposure and development in ma-D 525 developer, the waveguide patterns were defined on the sample. The Cr layer was etched by chlorine based inductively coupled plasma (ICP), and the  $\text{SiO}_2$  layer was etched by fluorine based reactive ion etching (RIE). Then, the exposed  $\beta\text{-Ga}_2\text{O}_3$  layer was removed by chlorine based ICP.<sup>17</sup> For the purpose of device protection and lower scattering loss,  $2\ \mu\text{m}$  PECVD  $\text{SiO}_2$  was deposited on the sample to cover the waveguides. Finally, the cross sections of the waveguides were exposed with a diamond blade cut, and diamond grind papers were employed to polish the cross sections to  $0.1\ \mu\text{m}$  grade, which enhanced the light coupling efficiency. Figures 1(b) and 1(c) show the representative scanning electron microscope (SEM) images of the  $\beta\text{-Ga}_2\text{O}_3$  waveguides before and after the optimization of ICP etching process, and the key ICP etching parameters were summarized in Table I. The original ICP etching recipe was chosen according to the previous research of chlorine based ICP.<sup>18</sup> However, the high  $\text{BCl}_3$  gas flow and ICP power caused the high plasma density, which resulted in extra etching perpendicular to sidewalls as identified in Fig. 1(b).

Figure 2(a) presents the propagation loss measurement system adopted in this work. Four different incident light wavelengths were chosen in the UV-NIR spectral:  $810\ \text{nm}$ ,  $633\ \text{nm}$ ,  $526\ \text{nm}$ , and  $400\ \text{nm}$ . The  $810\ \text{nm}$  wavelength was provided by a Ti:Sapphire laser

TABLE I. Key ICP parameters for unoptimized and optimized ICP etching recipe.

Etching recipe	ICP	Bias	Pressure	$\text{BCl}_3/\text{Ar}$	DC
Unoptimized	800 W	200 W	5 mtorr	50/5 sccm	290 V
Optimized	400 W	200 W	5 mtorr	20/5 sccm	330 V

with  $100\ \text{fs}$  pulse width and  $82\ \text{MHz}$  repetition rate. The latter three wavelengths were provided by three continuous-wave (CW) diode lasers. The waveguide mode was kept in fundamental TM polarization within this study. The incident light was focused by the objective lens and then coupled into the  $\beta\text{-Ga}_2\text{O}_3$  waveguide sample, which was mounted on a XYZ three-dimensional translation stage for precision alignment. When the guide mode was propagating along the waveguide, a linear CMOS camera was located above the sample to record the top scattered light, which can represent the light power transmitting in the waveguides after analysis in a computer. A linear regression of least squares fitting was applied on those scatter plots, the slope of which yields the power loss coefficient. This method is simple, accurate, and nondestructive, and has less requirements to coupling efficiency,<sup>19</sup> compared with other techniques.<sup>20,21</sup> Figure 2(b) shows the refractive indexes of  $\text{Ga}_2\text{O}_3$ (core), sapphire (substrate), and  $\text{SiO}_2$  (cladding), which suggests that the core-cladding structure is feasible

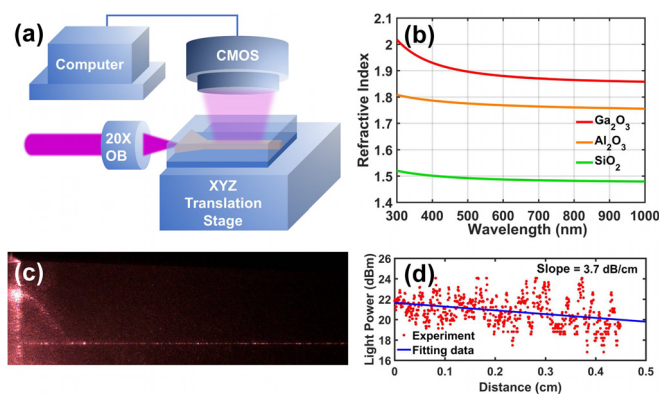


FIG. 2. (a) Schematic of the optical measurement system used in this study. (b) Refractive index of  $\text{Ga}_2\text{O}_3$ (core),  $\text{Al}_2\text{O}_3$ (substrate), and  $\text{SiO}_2$ (cladding). (c) Top image captured by the linear CMOS camera of a  $\beta\text{-Ga}_2\text{O}_3$  waveguide with  $1.5\ \mu\text{m}$  width at  $810\ \text{nm}$  wavelength. (d) Experimental data and regression analysis of a  $\beta\text{-Ga}_2\text{O}_3$  waveguide with  $3.7\ \text{dB/cm}$  loss.

within the UV–NIR spectra region. Figures 2(c) and 2(d) provide a typical recorded image from a linear CMOS camera during measurement and the extracted out-scattered light.

An objective lens ( $\times 20$ , 0.4 NA, 9 mm focal length) was used to inject the input laser beam into the taper structure to increase the coupling efficiency, as illustrated in Fig. 2(a). The radius of spot size is computed to be  $1.27 \mu\text{m}$  at the focal length. The taper structure has a width of  $7 \mu\text{m}$  at the beginning and gradually narrows to the width of the waveguides in 1 mm length. We simulate the transmission of TM mode in this taper structure using the finite-difference time-domain method. The coupling loss at the entrance is 1.71 dB. And the coupling of taper structure is less than 1.01 dB. Therefore, the total coupling loss is estimated to be less than 3 dB.

The fabricated  $\beta\text{-Ga}_2\text{O}_3$  waveguides with different widths from 0.5 to  $1.75 \mu\text{m}$  (same heights of  $1 \mu\text{m}$ ) were fabricated, and their propagation losses were summarized in Fig. 3(a). Overall, the propagation losses increased with decreasing widths and wavelengths, which is consistent with expectations. The minimum loss of 3.7 dB/cm was achieved for a waveguide with  $1.5 \mu\text{m}$  width and 810 nm wavelength. The transmission spectrum of  $\beta\text{-Ga}_2\text{O}_3$  indicates a high transmission in the visible spectral with an absorption edge at around 260 nm (253 nm for  $\vec{E} \parallel \vec{b}$  and 270 nm for  $\vec{E} \parallel \vec{c}$ ),<sup>22</sup> which is far away from the visible spectra. This suggests that the intrinsic material absorption is negligible for  $\beta\text{-Ga}_2\text{O}_3$  in the UV–NIR spectra. Other loss mechanisms such as the nonlinear two-photon absorption (TPA) and scattering may be the major contributors to the propagation loss in  $\beta\text{-Ga}_2\text{O}_3$  waveguides, which are discussed as follows.

Two-photon absorption becomes significant when the photon energy reaches half of bandgap energy. To estimate the TPA loss, the TPA coefficients at different wavelengths were theoretically calculated using the following equations:<sup>14,23</sup>

$$\beta(\omega) = K \frac{\sqrt{E_p}}{n_0^2 E_g^3} F_2 \left( \frac{\hbar\omega}{E_g} \right), \quad (1)$$

$$F_2(x) = \frac{(2x - 1)^{3/2}}{(2x)^5}, \quad (2)$$

where  $E_g$  is the bandgap energy of  $\beta\text{-Ga}_2\text{O}_3$  and  $E_p = 2 |\vec{p}_{vc}|^2 / m_0$ , which is obtained using  $\vec{k} \cdot \vec{p}$  theory.  $n_0$  is the refractive index of  $\beta\text{-Ga}_2\text{O}_3$ ,  $\omega$  is the light frequency, and  $K$  is a material-independent constant, which has a value of  $K = 1940$  in units such that  $\beta$  is in cm/GW, and  $E_g$  and  $E_p$  are in electron volts. The inset in Fig. 3(b) shows the wavelength dependence of TPA coefficient for  $\beta\text{-Ga}_2\text{O}_3$ , which is consistent with experimental results.<sup>14</sup> When the incident light wavelength is longer than 510 nm, the energy of two photons is not able to excite an electron to the conductive band, and the TPA coefficient is reduced to zero. Equation (3) gives the decay of light intensity  $I$ , where  $\alpha$  is the linear loss coefficient that resulted from scattering and material absorption and  $\beta$  is the TPA coefficient. The second term in Eq. (3) was used to calculate TPA losses. The waveguide light intensity profile  $I(x,y)$  of fundamental TM mode was calculated with a finite-difference method and then applied to Eq. (4) to calculate the absorbed light power in unit length  $L_0$ .<sup>24</sup>

$$dI/dz = -\alpha I - \beta I^2, \quad (3)$$

$$P = \int_0^{L_0} \int_{-\infty}^{+\infty} \int_{-\infty}^{+\infty} (-\beta I^2) dx dy dz. \quad (4)$$

Figure 3(b) shows the calculated TPA losses of a  $\beta\text{-Ga}_2\text{O}_3$  waveguide of  $1.0 \mu\text{m}$  width at CW TM mode at different wavelengths and input powers. A coupling loss of 3 dB was applied in the calculation to account for the input power loss when the laser light was injected into

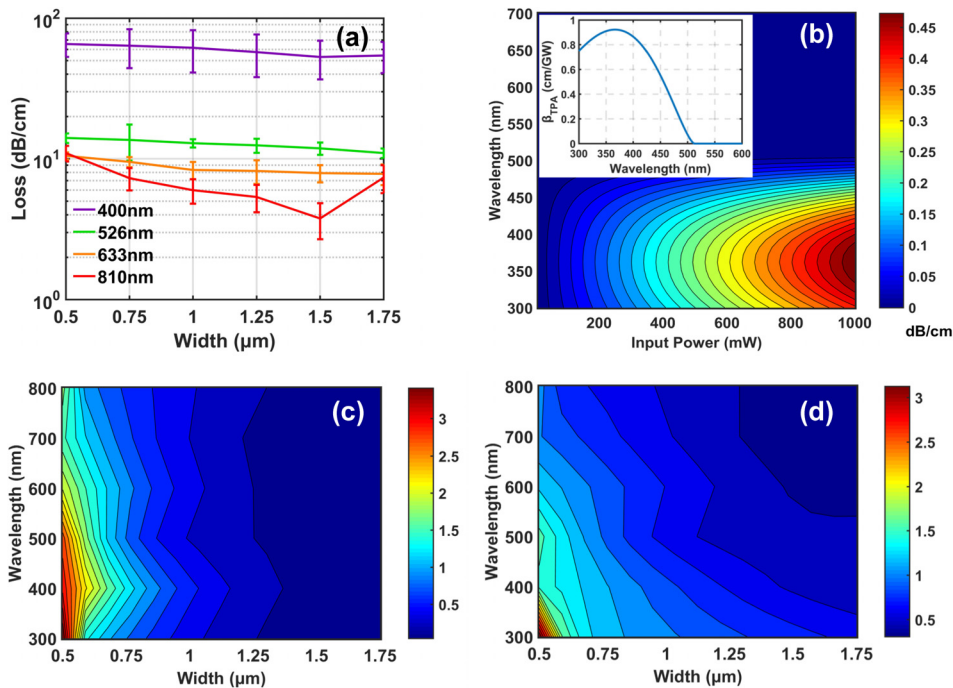


**FIG. 3.** (a) Measured propagation loss of  $\beta\text{-Ga}_2\text{O}_3$  waveguides with different widths at different wavelengths. (b) Calculated TPA loss for  $\beta\text{-Ga}_2\text{O}_3$  waveguides at different wavelengths and different input powers (inset: theoretical TPA coefficients). (c) Calculated sidewall scattering loss for  $\beta\text{-Ga}_2\text{O}_3$  waveguides. (d) Calculated top surface scattering loss for  $\beta\text{-Ga}_2\text{O}_3$  waveguides.



the waveguides. It is found that the TPA loss has a strong dependence on the input power, and the TPA loss values become significant at high powers and at wavelengths shorter than 500 nm. Since the input power in the experiment system was limited under 100 mW, there was only an imperceptible TPA loss of the  $\beta$ -Ga<sub>2</sub>O<sub>3</sub> waveguide devices reported in this work. However, it is still worth noting that if the waveguides work under pulsed laser conditions, the TPA loss will become significant. Assuming the same input light power and coupling loss in this calculation, the maximum light intensity ( $\sim 10^{12}$  W/cm<sup>2</sup>) of a pulsed laser (assuming pulse width of 400 ps and repetition rate of 10 kHz) is  $10^4$  times larger than the light intensity ( $\sim 10^8$  W/cm<sup>2</sup>) of a CW laser. Because of the intensity dependence, the TPA loss will become one of the major contributing factors for the propagation loss in  $\beta$ -Ga<sub>2</sub>O<sub>3</sub> waveguides under pulsed laser conditions.

For the scattering loss, three loss mechanisms are discussed for  $\beta$ -Ga<sub>2</sub>O<sub>3</sub> waveguides, i.e., top surface, sidewall, and bulk scattering. The top surface scattering and sidewall scattering are influenced by the roughness of top surface and sidewall, respectively. Both of them are also governed by the refractive index contrast between the waveguide material and the cladding material. Higher refractive index contrast will cause higher scattering losses.<sup>25,26</sup> The top surface roughness was mainly determined by the MOCVD process. The sidewall roughness was mainly caused by different etching rates of crystal grains with different crystalline orientations.

To properly model the scattering losses, the volume current method (VCM) was applied.<sup>27,28</sup> The roughness was decomposed into an array of unit nonidealities, and each nonideality was treated as “volume current sources.” By integrating the far-field radiated power from the volume current source and applying proper array factors, the total loss in dB/cm can be estimated. Using the dyadic Green’s function derived from previous work,<sup>27,28</sup> the electric field of a single dislocation can be calculated using the following equation:

$$\vec{E}(\vec{r}_c) = i\omega\mu \iiint \vec{G}(\vec{r}_c, \vec{r}_c') \vec{J}(\vec{r}_c') d\vec{V}', \quad (5)$$

where  $\vec{r}_c$  is the displacement vector of electric field,  $\vec{r}_c'$  is the displacement vector of volume current source,  $\mu$  is the permeability constant,  $\omega$  is the angular frequency of the incident light,  $\vec{G}(\vec{r}_c, \vec{r}_c')$  is the corresponding Green’s function, and  $\vec{J}(\vec{r}_c')$  is the volume current density. The far-field Poynting vector and the corresponding radiated light power can be obtained using the following equations:

$$\vec{S} = \vec{r} \frac{\omega n_1 k_0}{2\mu} |\vec{r} \times \vec{E}|^2, \quad (6)$$

$$P = \oint (\vec{S} \cdot \vec{r}) dA, \quad (7)$$

where  $n_1$  is the refractive index of the waveguide material and  $k_0$  is the free-space wavenumber. After applying the array factors<sup>27</sup> to the radiated light power of a unit nonideality, the total radiated power per unit length of the waveguide can be calculated using the following equations:

$$\vec{R}(\Omega) = 2\sigma^2 L_c / (1 + L_c^2 \Omega^2), \quad (8)$$

$$P/2L = 2\oint (\vec{S} \cdot \vec{r}) \vec{R}(\beta - n_c k_0 \cos \theta) dA, \quad (9)$$

where  $\sigma$  is the roughness,  $L_c$  is the correlation length that is set as 100 nm for simplicity,  $n_c$  is the refractive index of cladding material,  $\beta$

is the modal propagation constant, and the integration in Eq. (9) was in polar coordinates.

With an estimation of 10 nm sidewall roughness, assuming TM mode operation and waveguides height of 1  $\mu$ m, the scattering losses of sidewall and top surface of a  $\beta$ -Ga<sub>2</sub>O<sub>3</sub> waveguide were calculated and the results are shown in Figs. 3(c) and 3(d). Due to the “squeezed out” effect, waveguides with smaller dimension exhibit larger sidewall scattering loss, specifically when the width is narrower than 750 nm. On the other hand, the scattering losses are also sensitive to wavelengths. The waveguides under UV light exhibit stronger scattering loss compared with those under red light. This wavelength dependence is one of the main reasons to the dramatic increase in propagation losses of  $\beta$ -Ga<sub>2</sub>O<sub>3</sub> waveguides at UV spectral. It should be noted that the refractive index of  $\beta$ -Ga<sub>2</sub>O<sub>3</sub> ( $n \sim 1.85$ ) is relatively small compared with other III-N materials such as GaN ( $n \sim 2.35$ ) and AlN ( $n \sim 2.12$ ). Since the scattering loss is proportional to the contrast of the dielectric constants between the core and cladding materials ( $\Delta\epsilon$ ),  $\beta$ -Ga<sub>2</sub>O<sub>3</sub> is intrinsically less vulnerable to scattering losses and is ideal for high quality resonators in the UV–NIR spectral wavelengths. The appropriate index of  $\beta$ -Ga<sub>2</sub>O<sub>3</sub> also allows single mode operation in the relative larger waveguide dimensions, which is promising for the applications in on-chip high speed optical interconnections.

During the MOCVD growth, due to the large lattice mismatch between  $\beta$ -Ga<sub>2</sub>O<sub>3</sub> and sapphire, a large density of defects is expected in the  $\beta$ -Ga<sub>2</sub>O<sub>3</sub> films, such as grain boundaries and threading dislocations (typically  $10^8$ – $10^{10}$  cm<sup>-2</sup> defect density<sup>29</sup>). The bulk scattering loss induced by bulk defects can be calculated by removing the TPA loss, top surface scattering loss, and sidewall scattering loss from the total losses. Table II provides the contributions from each loss mechanism for three cases: case (A) width = 1.5  $\mu$ m,  $\lambda$  = 810 nm; case (B) width = 0.5  $\mu$ m,  $\lambda$  = 810 nm; case (C) width = 1.5  $\mu$ m,  $\lambda$  = 526 nm. The impact of TPA is minimum at these wavelengths due to the wide bandgap of  $\beta$ -Ga<sub>2</sub>O<sub>3</sub>. For case (A), the bulk scattering is responsible for the total loss due to the relatively large waveguide width. For case (B), the sidewall scattering dominates due to the overlapping between the optical mode and the sidewalls. For case (C) that has a shorter wavelength than case (A), a significant increase in total loss was obtained. This is the result from the boost of bulk scattering, which has a strong wavelength dependence. These analyses implied that the smooth sidewall roughness and better crystal quality are critical for achieving high performance low-loss  $\beta$ -Ga<sub>2</sub>O<sub>3</sub> waveguides.

Finally, compared with the state-of-the-art high-index-contrast integrated waveguides in the UV–NIR spectral region using other materials such as AlN ( $\sim 2.36$  dB/cm at 905 nm,  $\sim 8$  dB/cm at 390 nm),<sup>30,31</sup> the  $\beta$ -Ga<sub>2</sub>O<sub>3</sub> platform demonstrated comparable performance, and we foresee large space for further development of the  $\beta$ -Ga<sub>2</sub>O<sub>3</sub> technology. For example, the surface roughness for  $\beta$ -Ga<sub>2</sub>O<sub>3</sub> is 8.4 nm, which is very large compared to the typical roughness value in our materials such as GaN or AlN from optimized MOCVD process ( $< 3$  nm). The MOCVD process for the Ga<sub>2</sub>O<sub>3</sub> growth can be further optimized, which can greatly improve the top surface roughness and bulk inhomogeneities of the Ga<sub>2</sub>O<sub>3</sub> waveguide. It is also reported that the thermal annealing at 1000 °C can help us to improve the material quality of Ga<sub>2</sub>O<sub>3</sub>.<sup>32</sup> Bulk scattering can also be minimized by improving the crystalline quality. The roughness of sidewall is expected to decrease after further optimizations on the etching recipe.

**TABLE II.** Contributions of different loss mechanisms to the total propagation losses for  $\beta$ -Ga<sub>2</sub>O<sub>3</sub> waveguides (unit of dB/cm).

	Total loss	TPA	Top surface scattering	Sidewall scattering	Bulk scattering
(A) Width = 1.5 $\mu$ m $\lambda$ = 810 nm	3.76	0	0.38	0.06	3.32
(B) Width = 0.5 $\mu$ m $\lambda$ = 810 nm	10.95	0	1.07	7.16	1.40
(C) Width = 1.5 $\mu$ m $\lambda$ = 526 nm	11.85	0	0.49	0.60	10.76

In summary, we fabricated a low loss  $\beta$ -Ga<sub>2</sub>O<sub>3</sub> waveguide. A propagation loss of 3.7 dB/cm was obtained at the wavelength of 810 nm, which is promising for a wide variety of optical applications. Combined with theoretical simulations, various loss mechanisms from two-photon absorption, sidewall scattering, top surface scattering, and bulk scattering were discussed for  $\beta$ -Ga<sub>2</sub>O<sub>3</sub> waveguides, and their contributions to the total optical loss were estimated. This work provides valuable information for the fabrication of optical devices based on Ga<sub>2</sub>O<sub>3</sub> material, which is promising for applications in on-chip high speed interconnections and UV–NIR nonlinear optics.

This work is partially supported by the Army Research Office (ARO) PECASE Grant No. W911NF-19-1-0089, and the ARO DURIP Grant No. W911NF-19-1-0129, monitored by Dr. Michael Gerhold. We gratefully acknowledge the use of facilities within NanoFab, John M. Cowley Center for High Resolution Electron Microscopy (CHREM), Goldwater Materials Science Facility (GMSF), Ultra-Fast Laser Facility and Ning's Nanophotonics Lab in Arizona State University.

## REFERENCES

- R. Konoike, K. Suzuki, S. Namiki, H. Kawashima, and K. Ikeda, *Opt. Express* **27**, 10332 (2019).
- W. Bogaerts and L. Chrostowski, *Laser Photonics Rev.* **12**, 1700237 (2018).
- D. D. Hickstein, H. Jung, D. R. Carlson, A. Lind, I. Coddington, K. Srinivasan, G. G. Ycas, D. C. Cole, A. Kowligy, C. Fredrick, S. Droste, E. S. Lamb, N. R. Newbury, H. X. Tang, S. A. Diddams, and S. B. Papp, *Phys. Rev. Appl.* **8**, 014025 (2017).
- H. Zhao, B. Kuyken, S. Clemmen, F. Leo, A. Subramanian, A. Dhakal, P. Helin, S. Severi, E. Brainis, G. Roelkens, and R. Baets, *Opt. Lett.* **40**, 2177 (2015).
- S. H. Lee, D. Y. Oh, Q.-F. Yang, B. Shen, H. Wang, K. Y. Yang, Y.-H. Lai, X. Yi, X. Li, and K. Vahala, *Nat. Commun.* **8**, 1295 (2017).
- K. H. Li, W. Y. Fu, Y. F. Cheung, K. K. Y. Wong, Y. Wang, K. M. Lau, and H. W. Choi, *Optica* **5**, 564 (2018).
- S. Romero-García, F. Merget, F. Zhong, H. Finkelstein, and J. Witzens, *Opt. Express* **21**, 14036 (2013).
- P. Muellner, E. Melnik, G. Koppitsch, J. Kraft, F. Schrank, and R. Hainberger, *Procedia Eng.* **120**, 578 (2015).
- A. L. Gaeta, M. Lipson, and T. J. Kippenberg, *Nat. Photonics* **13**, 158 (2019).
- J. F. Bauters, M. J. R. Heck, D. John, D. Dai, M.-C. Tien, J. S. Barton, A. Leinse, R. G. Heideman, D. J. Blumenthal, and J. E. Bowers, *Opt. Express* **19**, 3163 (2011).
- M. Higashiwaki, K. Sasaki, A. Kuramata, T. Masui, and S. Yamakoshi, *Appl. Phys. Lett.* **100**, 013504 (2012).
- M. Higashiwaki, K. Sasaki, H. Murakami, Y. Kumagai, A. Koukita, A. Kuramata, T. Masui, and S. Yamakoshi, *Semicond. Sci. Technol.* **31**, 034001 (2016).
- H. Peelaers and C. G. Van de Walle, *Phys. Status Solidi B* **252**, 828 (2015).
- H. Chen, H. Fu, X. Huang, J. A. Montes, T.-H. Yang, I. Baranowski, and Y. Zhao, *Opt. Express* **26**, 3938 (2018).
- S. Nakagomi and Y. Kokubun, *J. Cryst. Growth* **349**, 12 (2012).
- Z. Feng, A. F. M. Anhar Uddin Bhuiyan, M. R. Karim, and H. Zhao, *Appl. Phys. Lett.* **114**, 250601 (2019).
- S. J. Pearton, J. Yang, P. H. Cary, F. Ren, J. Kim, M. J. Tadjer, and M. A. Mastro, *Appl. Phys. Rev.* **5**, 011301 (2018).
- J. Yang, S. Ahn, F. Ren, S. Pearton, R. Khanna, K. Bevin, D. Geerapuram, and A. Kuramata, *J. Vac. Sci. Technol., B* **35**, 031205 (2017).
- F. Wang, *Opt. Eng.* **47**, 024602 (2008).
- P. Neutens, M. Rutowska, W. Van Roy, R. Jansen, F. Buja, and P. Van Dorpe, *ACS Photonics* **5**, 2145 (2018).
- J. Wei, X. F. Xu, Y. Ding, Z. H. Kang, Y. Jiang, and J. Y. Gao, *Opt. Lasers Eng.* **45**, 419 (2007).
- N. Ueda, H. Hosono, R. Waseda, and H. Kawazoe, *Appl. Phys. Lett.* **71**, 933 (1997).
- M. Sheik-Bahae, D. C. Hutchings, D. J. Hagan, and E. W. Van Stryland, *IEEE J. Quantum Electron.* **27**, 1296 (1991).
- T. K. Liang, H. K. Tsang, I. E. Day, J. Drake, A. P. Knights, and M. Asghari, *Appl. Phys. Lett.* **81**, 1323 (2002).
- F. P. Payne and J. P. R. Lacey, *Opt. Quantum Electron.* **26**, 977 (1994).
- J. P. R. Lacey and F. P. Payne, *IEE Proc. J Optoelectron.* **137**, 282 (1990).
- T. Barwicz and H. A. Haus, *J. Light. Technol.* **23**, 2719 (2005).
- H. Chen, H. Fu, J. Zhou, X. Huang, T.-H. Yang, K. Fu, C. Yang, J. A. Montes, and Y. Zhao, *Opt. Express* **27**, 17262 (2019).
- Q. Feng, L. Huang, G. Han, F. Li, X. Li, L. Fang, X. Xing, J. Zhang, W. Mu, Z. Jia, D. Guo, W. Tang, X. Tao, and Y. Hao, *IEEE Trans. Electron Devices* **63**, 3578 (2016).
- X. Liu, A. W. Bruch, Z. Gong, J. Lu, J. B. Surya, L. Zhang, J. Wang, J. Yan, and H. X. Tang, *Optica* **5**, 1279 (2018).
- S. Zhu, Q. Zhong, T. Hu, Y. Li, Z. Xu, Y. Dong, and N. Singh, in *Opt. Fiber Commun. Conf. 2019 (OSA, Washington, D.C., 2019)*, p. W2A.11.
- J.-H. Park, R. McClintock, A. Jaud, A. Dehzangi, and M. Razeghi, *Appl. Phys. Express* **12**, 095503 (2019).